https://doi.org/10.5194/egusphere-2025-3602
Preprint. Discussion started: 11 August 2025

Real-Time Measurement of NO and NH_3 Concentration Variations Using Direct Absorption Spectroscopy in the Smog Chamber to Analyze NH_4NO_3 Photochemical Formation Characteristics

Nakwon Jeong[1,2], Seungryong Lee[1,2], Daehae Kim[1], Miyeon Yoo[1], Soonho Song[2,*], Changyeop Lee[1,*]

[1]Korea Institute of Industrial Technology (KITECH), 89 Yangdaegiro-gil, Cheonan, 31056, Republic of Korea
[2]Department of Mechanical Engineering, Yonsei University, 50 Yonsei-ro, Seoul, 03722, Republic of Korea

Correspondence to: Soonho Song (soonhosong@yonsei.ac.kr), Changyeop Lee (cylee@kitech.re.kr)

Abstract. In urban atmospheric chemistry, NOx and NH_3 in the atmosphere are major species participating in the secondary aerosol formation process, causing severe environmental problems such as decreased visibility and acid rain. In order to respond effectively to particulate matter problems, the correlation of precursors should be identified in detail. This study used UV-C light to convert gaseous substances into particulate substances in the small-scale smog chamber to simulate the photochemical reaction. The effects of several operating variables, such as UV-C light intensity, relative humidity, and initial concentrations of O_2, NO, and NH_3, on the NH_4NO_3 formation were investigated. Since atmospheric gas species are short-lived, they require a measurement technique with real-time and high sensitivity. Therefore, the concentrations of NO and NH_3 were measured using Direct Absorption Spectroscopy techniques in the wavenumber regions of 1926 and 6568 cm^{-1}, respectively. The DAS-measured concentrations of NO and NH_3 showed less than 3% deviation compared to certified reference gas concentrations in the 10 – 90 ppmv range. The results show that NO and NH_3 were converted over 98% when UV-C light intensity was 24W and relative humidity was about 30% at 1 atm, 296 K. It also showed that higher UV-C light intensity, O_3 concentration, and relative humidity induced higher conversion and secondary aerosol generation. In particular, it was experimentally confirmed that the secondary aerosol generation and growth process was greatly influenced by relative humidity.

1 Introduction

Aerosols in the atmosphere cause severe environmental and social issues by adversely affecting human health, disrupting solar radiation transfer, and influencing cloud formation (Zhang et al., 2015; Butt et al., 2016). Airborne aerosols are divided into two groups. Primary aerosols are emitted directly from various emission sources, and secondary aerosols are formed via homogeneous nucleation through physicochemical processes in the atmosphere. Precursor materials such as nitrate, sulfate, and NH_3 in the atmosphere are major species that participate in secondary aerosol formation and growth processes. NOx contributes to acid deposition and form atmospheric oxidants ozone and nitrate radical (Fuchs et al., 2010). NH_3 increases natural water and soil acidity, providing excessive nitrogen injection into the ecosystem (Stevens et al., 2010). Sulfate or nitrate,

https://doi.org/10.5194/egusphere-2025-3602
Preprint. Discussion started: 11 August 2025

which accounts for a large proportion of the contribution to airborne aerosol production, leads to localized cooling by scattering solar radiation (Adopted, 2014). It can also influence the macroscopic and microscopic physical properties of clouds and affect precipitation variability by providing a source of cloud condensation nuclei or ice nuclei (Tao et al., 2012).

Ammonium nitrate (NH_4NO_3) aerosol is formed through the chemical reaction between gaseous NH_3 and nitric acid (HNO_3) in the atmosphere and is highly dependent on atmospheric chemistry and meteorological conditions. Under high relative humidity, it can exist as an aqueous solution of NH_4^+ and NO_3^-, while under low relative humidity, it often exists as solid particles (Bauer et al., 2007). Additionally, it is highly sensitive to temperature, forming particulate NH_4NO_3 at lower temperatures and decomposing into gaseous NH_3 and HNO_3 as the temperature rises (Stelson and Seinfeld, 1982). The dominant formation pathways of HNO_3, a major precursor for NH_4NO_3 formation, are influenced by sunlight availability. During the day, it is produced through the oxidation of NOx by OH radicals generated by photolysis under sunlight, whereas at night, it can form via the hydrolysis reaction of dinitrogen pentoxide (N_2O_5) (Kelly et al., 2018).

Numerous researchers measured and simulated atmospheric pollutants to study in detail the interactions between these precursors and various atmospheric conditions (Khoder, 2002; Han et al., 2011; Zhao et al., 2016; Kelly et al., 2018). However, since many factors, such as meteorological conditions and pollutant emission rates, cannot be artificially controlled, it is difficult to determine the cause of secondary pollutants by monitoring only the concentration of reactants and products in complex photochemical chemistry (Lee et al., 2009). Consequently, studies have been conducted actively using smog chambers that can study the nucleation, hygroscopic growth, and extinction of specific compounds in an environment isolated from the outside. Spicer (1983) studied in a large-scale smog chamber (17.3 m^3) to understand the atmospheric NOx conversion and the relationship between nitrates, hydrocarbons, and NOx precursors. Besides, studies were conducted to investigate the secondary inorganic aerosol (SIA) formation kinetics in an outdoor simulation chamber and to investigate the effects of NOx and NH_3 on secondary organic aerosol (SOA) formation from photooxidation of toluene in the indoor chamber (Behera and Sharma, 2011; Qi et al., 2020).

In most smog chamber studies, gaseous precursor concentrations are typically measured using methods such as chemiluminescence, FTIR, and NDIR. However, these techniques have limited temporal resolution due to sampling and analysis delays, which makes them less suitable for capturing the rapid fluctuations characteristic of photochemical reactions. Furthermore, since these methods require gas extraction and handling, they may alter the chemical composition or dynamics of reactive species prior to measurement. To overcome these limitations, Direct Absorption Spectroscopy (DAS) offers a clear advantage by enabling real-time, in situ measurements without disturbing the gas-phase reactions (So et al., 2022). DAS is highly sensitive and capable of tracking concentration variations in real time, providing a more accurate analysis of photochemical processes in complex atmospheric conditions. In this study, DAS allowed for accurate and interference-free NO measurements at 1926 cm^{-1} and NH_3 at 6568 cm^{-1}, facilitating a deeper understanding of their roles in secondary aerosol formation. These measurements offer significant insights into the reaction dynamics of NO, NH_3, and other atmospheric constituents, such as O_3 and OH radicals, that contribute to the formation of NH_4NO_3. Thus, the sensitive and real-time measurements enabled by DAS contribute significantly to capturing rapid concentration fluctuations under complex

https://doi.org/10.5194/egusphere-2025-3602
Preprint. Discussion started: 11 August 2025

atmospheric conditions. This approach enhances the understanding of photochemical processes and provides valuable insights into the interactions of various atmospheric variables, improving the accuracy of aerosol formation studies.

Although numerous studies have explored aerosol formation mechanisms, significant uncertainties remain regarding how environmental conditions such as UV intensity, humidity, and temperature affect the nucleation and growth of secondary aerosols. In particular, the photochemical conversion of NO and NH_3 to NH_4NO_3 under controlled atmospheric conditions is not yet fully understood. To address these gaps, we conducted real-time laser absorption spectroscopy experiments in a small-scale smog chamber to investigate how precursor gas concentrations and environmental parameters influence NH_4NO_3 formation dynamics. Real-time NO and NH_3 measurements using DAS enabled a comprehensive analysis of their roles in the formation process. The results provide new insights into the influence of UV light intensity, relative humidity, and gas concentrations on the reaction kinetics and mechanisms, offering a clearer understanding of the environmental conditions that promote or inhibit secondary aerosol formation. This approach also helps identify dominant reaction pathways and key variables that regulate NH_4NO_3 production, contributing to the development of more accurate predictive models for atmospheric aerosol behavior.

2 Line selection

To ensure accurate detection of NO and NH_3 using DAS, absorption lines were selected based on line strength and minimal spectral interference under the experimental conditions. Therefore, spectral simulations were performed to identify optimal lines with strong absorption and minimal interference from background species such as H_2O.

Fig. 1(a) shows the simulation results under experimental conditions in the spectral range of 1910 to 1940 cm^{-1} under standard temperature and pressure (STP). Spectral simulations confirmed that the NO absorption feature near 1926 cm^{-1} offer sufficient sensitivity and minimal overlap with interfering species such as H_2O. Similarly, Figure 1(b) presents the simulated absorbance spectra of NH_3 and H_2O in the 6560 to 6580 cm^{-1} spectral range under STP. Among the accessible NIR lines, the absorption feature near 6568 cm^{-1} was chosen due to its relatively high line strength and minimal interference from adjacent NH_3 or H_2O transitions. Although its line strength is weaker than in the mid-IR, this was compensated by employing a multi-pass cell with a 25 m optical path length, enabling sufficient sensitivity for low-ppmv NH_3 detection. These choices ensure reliable quantification of NO and NH_3 in a multi-species mixture typical of photochemical reaction systems.

https://doi.org/10.5194/egusphere-2025-3602
Preprint. Discussion started: 11 August 2025

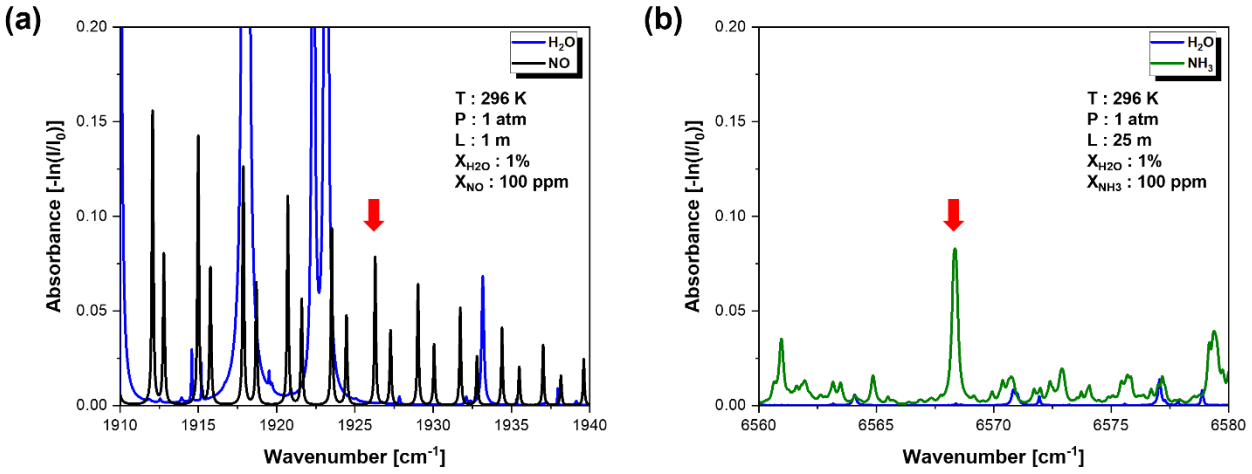

Figure 1: (a) simulated absorbance spectrum of X_{H2O} 1%, X_{NO} 100 ppmv in the 1910 to 1940 cm^{-1} spectral range, (b) simulated absorbance spectrum of X_{H2O} 1%, X_{NH3} 100 ppmv in the 6560 to 6580 cm^{-1} spectral range at 1atm, 296 K based on HITRAN2016 database (Gordon et al., 2017).

3 Experimental setup

3.1 Small-scale indoor smog chamber

This study investigated the real-time nucleation and hygroscopic growth of NH_4NO_3 by monitoring concentration variations of NO and NH_3 in a smog chamber under isolated conditions. The small-scale indoor smog chamber was designed with cylindrical quartz with a volume of ~ 3.85 L (7 cm in diameter, 100 cm in length) and a surface-area-to-volume ratio of ~ 1.75 m^{-1}. Quartz was selected as the chamber material due to its chemical inertness and stability under reactive gas conditions (Kim et al., 2024). To promote photochemical reactions efficiently, four UV-C ozone lamps (180 - 280 nm, peak at 253.7 nm; 35 cm, 14 W, Hansung Ultraviolet Company GHO436T5VH) were installed inside the chamber. UV-C was selected due to its short wavelength and high-energy photon output, which can induce specific reactions such as photolysis of NO_2 and decomposition of O_3. While UV-C light is not present under natural tropospheric conditions, it was intentionally employed in this study to enhance photolysis efficiency and accelerate reaction kinetics. This enabled clearer observation of precursor conversion as well as the nucleation and growth mechanisms of NH_4NO_3 within the smog chamber.

https://doi.org/10.5194/egusphere-2025-3602
Preprint. Discussion started: 11 August 2025

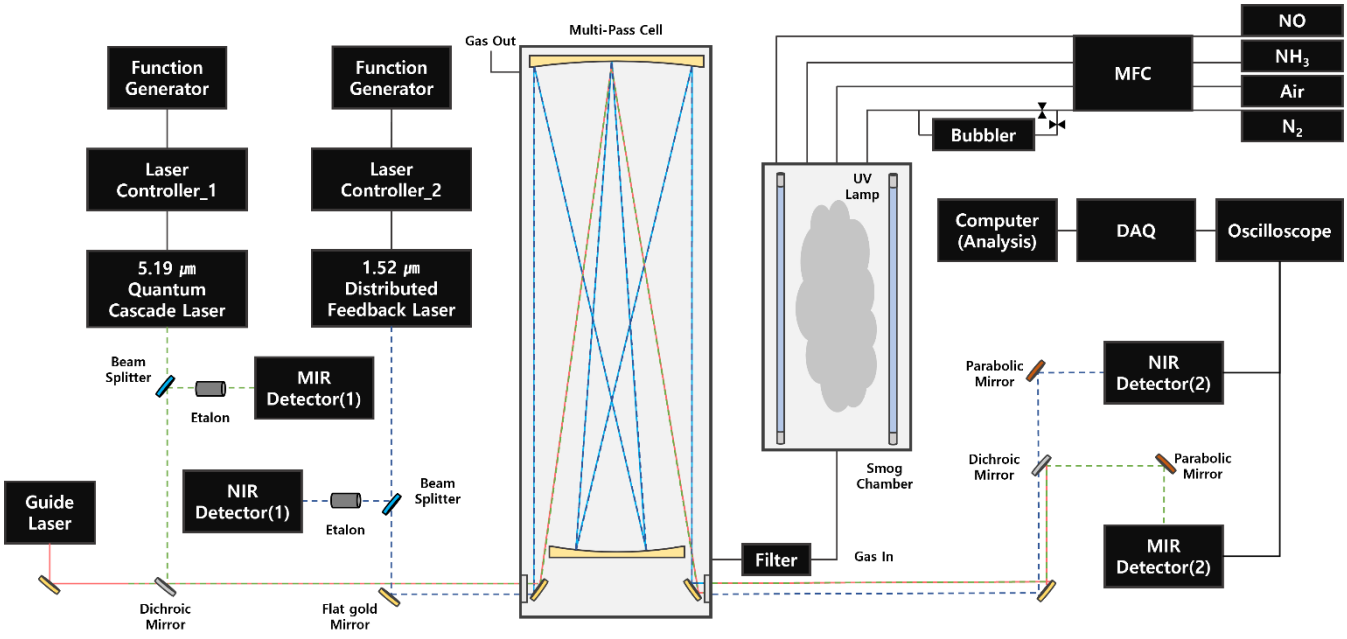

Figure 2: Schematic diagram of atmospheric smog simulation system for inducing photochemical reactions and an optical sensor system for measuring gaseous precursor concentrations; MFC: mass flow controller, DAQ: data acquisition, MIR: mid-infrared, NIR: near-infrared

Fig. 2 shows a schematic diagram of an overall experiment combining the atmospheric smog simulation system part to induce the photochemical reaction and the optical sensor system part to measure precursor concentration. The external environment is maintained at 1atm, 296 ± 2 K, and 30 to 60% relative humidity, which are typical conditions for atmospheric simulations. The experiment used purified air, high-purity N_2, and 300 ppmv of NO/N_2, NH_3/N_2 reference gas supplied through a calibrated mass flow controller (MFC). In order to control relative humidity in the chamber, high-purity N_2 was passed through the H_2O bubble generator heated to about 350 K and supplied to the chamber. When N_2 was injected at $2\ L/min$, the relative humidity was measured at 60%. The temperature in the chamber was maintained at 296 ± 2 K. To minimize adsorption at the gas line, the distance between the simulation chamber and the multi-pass cell was placed close, and all reactants were continuously flowed to ensure thorough mixing within the chamber. The polytetrafluoroethylene (PTFE) microporous membrane filter with a pore size of 1.0 μm was used to sample NH_4NO_3 formed by the photochemical reaction.

The experiments were conducted using ultra-high purity gases to ensure accuracy and minimize contamination. Specifically, 99.999% high-purity nitrogen and dry air were used as carrier gases, along with nitrogen-based calibration gases containing 300 ppmv NO and NH_3. The residence time of gas mixtures within the smog chamber was calculated using the chamber volume and the volumetric flow rate of incoming gases. For a smog chamber volume of 3.85 L and a total flow rate of 0.133 L/s, the residence time was approximately 28.9 seconds. This ensured sufficient interaction time for photochemical reactions under controlled conditions. To ensure the accuracy and reliability of the experimental results, cleaning and calibration procedures

https://doi.org/10.5194/egusphere-2025-3602
Preprint. Discussion started: 11 August 2025

were rigorously followed. High-purity N_2 was flushed through the chamber at a flow rate of 1 L/min for at least 1 hour before and after each experiment. This process effectively removed gas species adsorbed on the inner walls of the chamber, minimizing contamination and ensuring consistent initial conditions. All measurements were performed to confirm system stability and to eliminate potential biases prior to experimental runs. To minimize inlet losses to the white-type multi-pass cell, several measures were implemented. The distance between the simulation chamber outlet and the multi-pass cell inlet was reduced to approximately 0.3 m to prevent significant diffusion or adsorption of reactive gases along the transport path. All gas lines were made of materials with low adsorption properties, such as Fluorinated ethylene propylene (FEP), to reduce surface interactions. These precautions minimized potential losses and ensured that the measured gas concentrations accurately reflected the conditions inside the simulation chamber.

3.2 Laser sensor system setup

The optical sensor system can be divided into the laser transmitter and absorption signal receiver. The high heat load type quantum cascade (QC) laser of 1926 cm^{-1} spectral range (Alpes Lasers, Switzerland) and the butterfly 14 pin type of distributed feedback (DFB) laser of 6568 cm^{-1} spectral range (NTT Electronics, Japan) were installed as shown Fig. 2. The laser controllers (Arroyo Instruments 6310-QCL, ILX Lightwave LDC-3908) that apply a constant temperature and current was used to emit the laser with appropriate wavenumber. Here, the temperature and current of the laser controllers were verified to confirm the emitting selected spectral range using a wavemeter (HighFinesse Laser and Electronic Systems WS6-200) calibrated with a stabilized laser reference (HighFinesse Laser and Electronic Systems SLR 1532). 10 kHz ramp wave was applied using a function generator (Tektronix AFG31000) that regulates voltage and frequency. The light emitted from the laser was split at 9:1 by a beam splitter, and the minor light passed through the solid etalon to convert the time domain to the wavenumber domain. To compensate for the relatively weak absorption line strength of NH_3, a multi-pass cell with a length of 0.5 m and a total path length of 25 m was used. On the contrary, in the case of NO, the absorption line strength is stronger than that of NH_3, so the path length was aligned to 1 m. The two lasers were aligned by adjusting the angles at which they entered the multi-pass cell using a flat gold mirror and a dichroic mirror, respectively, to achieve the required path length. In the absorption signal receiver part shown in Fig. 2, the light that passed the multi-pass cell was focused through a parabolic mirror and then irradiated to the amplified photodetectors (Thorlabs PDAVJ8, PDA50B2) to minimize optical loss. The measured absorption signal can be visualized via oscilloscope (Teledyne WS3024z), and the signals acquired by the data acquisition (DAQ) system with 10 MS/s and analyzed using MATLAB.

3.3 Experimental conditions

The process of nucleation and hygroscopic growth of secondary aerosols by photochemical reactions in the atmosphere is significantly influenced by atmospheric conditions. These experiments were conducted to investigate the effect of each variable,

https://doi.org/10.5194/egusphere-2025-3602
Preprint. Discussion started: 11 August 2025

as aerosol formation and growth processes respond sensitively to UV light intensity, relative humidity, and concentrations of secondary aerosol precursors.

Gases were continuously supplied to the smog chamber for 90 seconds at a constant flow rate. UV-C lamps were turned on at 30 seconds and operated for a duration of 60 seconds, allowing for sufficient time to induce photochemical reactions. During this period, the variations in gas concentrations were measured in real time. Data acquisition was performed by averaging 1,000 individual measurements to generate one data point per second.

Table 1: Experimental conditions for photochemical reaction simulation.

Case		1	2	3	4	5
Mass flow rate [slpm]	NO (300 ppmv)	3	3	3	2 / 2.5 / 3 / 3.5 / 4	3
	NH_3 (300 ppmv)	3	3	3	3	2 / 2.5 / 3 / 3.5 / 4
	Purified Air	1	0 / 0.5 / 1 / 1.5 / 2	0 / 0.5 / 1 / 1.5 / 2	1	1
	N_2 (99.999%)	1	2 / 1.5 / 1 / 0.5 / 0	2 / 1.5 / 1 / 0.5 / 0	2 / 1.5 / 1 / 0.5 / 0	2 / 1.5 / 1 / 0.5 / 0
Humidified sample air		Unused	Unused	Used	Unused	Unused
No. of lamps used		1 / 2 / 3 / 4	2	2	2	2

The experimental conditions are summarized in Table 1. In Case 1, the number of UV-C lamps was adjusted to compare the concentration reduction and conversions of NO and NH_3 according to the UV light intensity. In Case 2, the mass flow rate of purified air and N_2 was controlled and measured to investigate the photochemical reaction of NO and NH_3 according to the concentration of O_2, and Case 3 was conducted to check the effect of relative humidity in the NH_4NO_3 formation by photochemical reactions. Through Cases 4 and 5, NH_4NO_3 formation was investigated as a function of NO and NH_3 mixing ratios.

4 Results and discussion

4.1 Accuracy of DAS sensor

The preliminary experiment evaluated the accuracy of NO and NH_3 concentration measurements. The experiment was conducted using the setup shown in Fig. 2, where the 6568 cm^{-1} laser beam was coupled into a White-type multi-pass cell providing an effective optical path length of 25 m, while the 1926 cm^{-1} laser beam was directed through a 1 m single-pass optical path. Under ambient temperature and pressure conditions, high-purity N_2 and 300 ppmv NO/N_2 and NH_3/N_2 reference gases were used. Target mixing ratios ranging from 10 to 90 ppmv were achieved by diluting the reference gases with pure N_2 using MFC. Fig. 3(a) and (b) illustrate the measured absorption spectra of NO and NH_3 at 90 ppmv, fitted using Voigt profiles. The residuals between the measured and fitted data are also shown to validate the fitting accuracy. To improve measurement accuracy when deriving concentrations via the DAS method, applying the Voigt profile to the absorption signals is essential before calculating the integrated absorbance area A_i to reduce noise. Fig. 3(c) and (d) show a strong linear relationship ($R^2 \approx$

https://doi.org/10.5194/egusphere-2025-3602
Preprint. Discussion started: 11 August 2025

185 0.999) between the concentrations set via calibrated MFCs and those measured by the DAS method, confirming the high accuracy and precision of the sensor. The error bars in the plots represent the standard deviation of three replicate measurements at each concentration level, including uncertainty associated with both signal variability and the dilution process through MFC control.

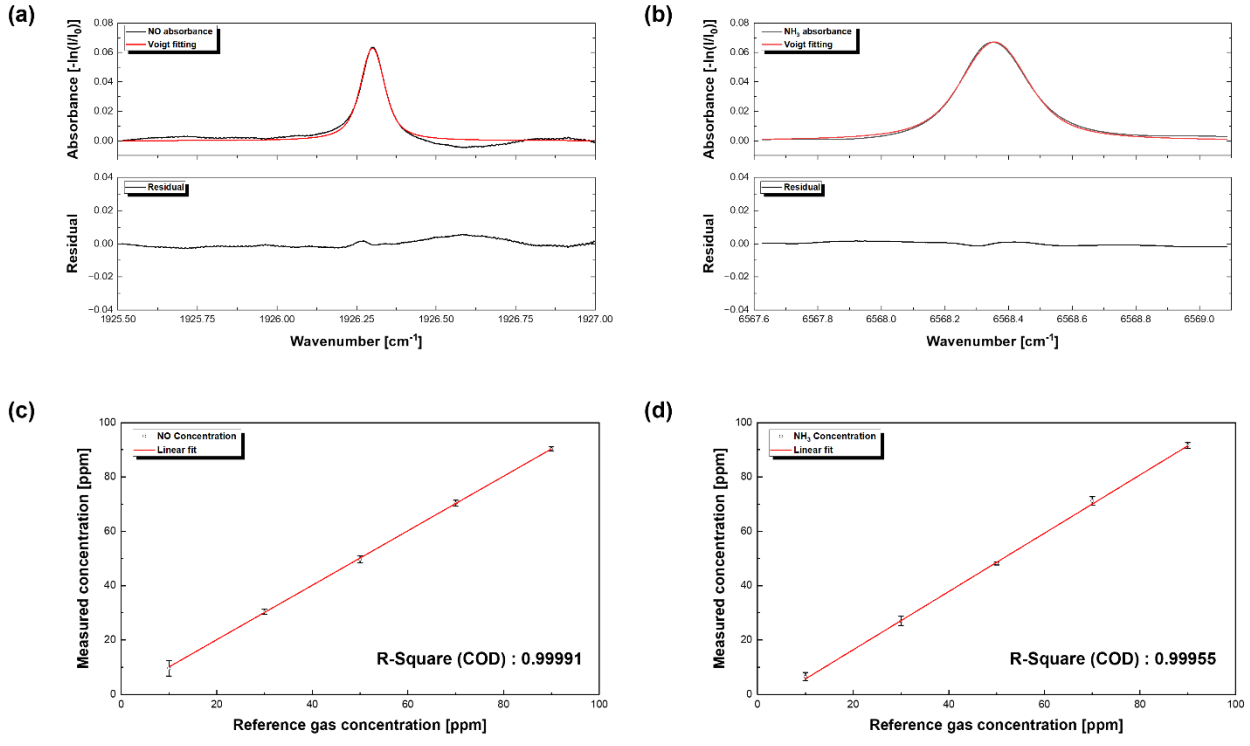

190

Figure 3: (a), (b) Absorption spectra of NO and NH_3 at 90 ppmv, respectively, fitted with Voigt profile and corresponding residuals, (c), (d) Linear relationships between the concentrations of NO and NH_3 set by MFCs. Error bars indicated the standard deviation from three replicate measurements, reflecting uncertainties from signal variability and MFC-based dilution.

4.2 Effect of UV light intensity on NH_4NO_3 formation

195 Since sunlight's light intensity varies depending on the weather or season and the reaction rate of precursors varies accordingly, research on the concentration variations of NO and NH_3 depending on light intensity should be conducted. Therefore, the number of UV-C lamps was changed to control light intensity when NO, NH_3, purified air, and N_2 have the constant mass flow rate, as shown in Case 1 of Table 1.

Fig. 4(a) and (b) show NO and NH_3 concentration graphs according to the number of applied UV-C lamps. The photochemical
200 reaction test, according to light intensity, was measured while continuously injecting gas for 90 seconds, and the UV-C lamps were operated for 30 to 90 seconds. In the case of NO, under the 14 W condition where one lamp was applied, it decreased by 69% to reach the steady-state for about 42 seconds. Furthermore, under the conditions where 4 of UV-C lamps applied, it

https://doi.org/10.5194/egusphere-2025-3602
Preprint. Discussion started: 11 August 2025

reached a steady-state after decreasing by 85% over approximately 35 seconds. These results suggest that OH radicals and O_3 were generated through the photolysis of H_2O and O_2 by UV-C light, enhancing the overall reaction rate under higher light intensity. Gaseous NH_3 decreased by about 47, 73, 85, and 94% as UV-C lamps increased. In the case of NO, the maximum NO reduction quantity is almost similar when the light intensity is 28 W or higher, whereas the reduced quantity of NH_3 tends to increase gradually. This is attributed to the increase in light intensity, as indicated by the $\cdot O + NO_2 \rightarrow O_2 + NO$ reaction, which leads to an increase in $\cdot O$, causing the decomposition of NO_2 into NO and O_2. Additionally, the increased decomposition of H_2O into OH radicals by higher light intensity is considered responsible for the conversion of NO_2 into HNO_3 as described in the $NO_2 + \cdot OH + M \rightarrow HNO_3 + M$ reaction.

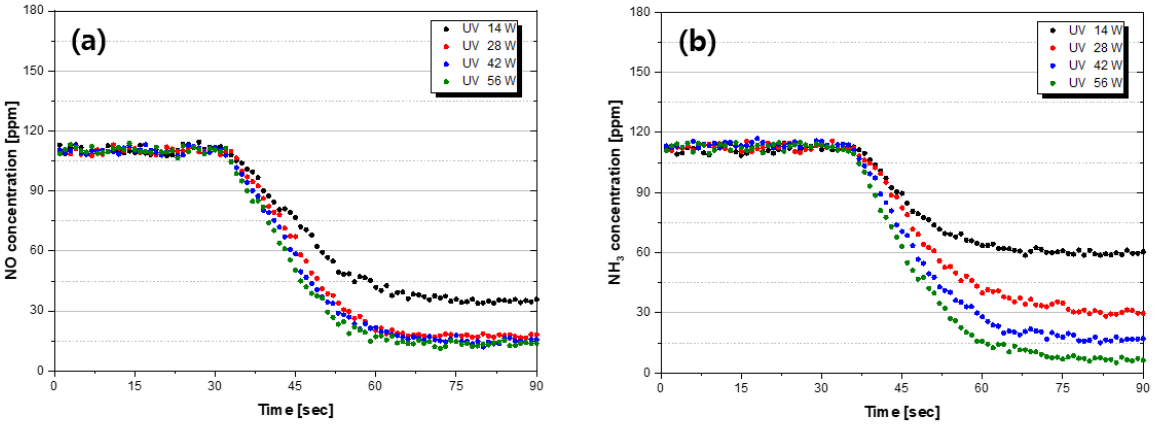

Figure 4: Time evolution of NO and NH_3 concentrations in NO, NH_3, O_2, and N_2 mixtures under different UV-C light intensities for Case 1 (see Table 1). (Black dot: 14W emitted from 1 UV-C lamp, red dot: 28W emitted from 2 UV-C lamps, blue dot: 42W emitted from 3 UV-C lamps, green dot: 56W emitted from 4 UV-C lamps)

From a temporal perspective, it was observed that there is a slight delay in the decrease of NO and NH_3 concentrations after UV light irradiation begins. This delay can be attributed to the time required for the reacted gases to travel from the chamber to the multi-pass cell. Here, the reaction start time represents when the initial concentration decreases by over 3%. The reaction of NO was faster than that of NH_3 because NO is reacted faster by O_3 and OH radicals, i.e., while NH_3 begins to react after HNO_3 is formed. In addition, its reaction rate is also considered to be slower than the rate at which NO is converted to NO_2 or $\cdot HONO$.

4.3 Effect of initial O_2 concentration on NH_4NO_3 formation

In the atmosphere, O_3 is generated through the photolysis of NO_2, and NO_2 is regenerated by reaction with NO, establishing a photostationary state equilibrium among O_3, NO, and NO_2 (Andersen et al., 2022). Also, highly reactive hydroperoxyl radical ($\cdot HO_2$) and peroxyl radical ($\cdot RO_2$) produced by volatile organic compounds (VOCs) oxidation convert NO to NO_2 (Carslaw

https://doi.org/10.5194/egusphere-2025-3602
Preprint. Discussion started: 11 August 2025

et al., 1999). In this sequence of reactions, RO_2 and HO_2 in the atmosphere determine the net production of ozone. Therefore, since the O_3 concentration increases in an environment where VOCs are emitted, it is necessary to study the process of NH_4NO_3 photochemical reactions according to various O_3 concentrations.

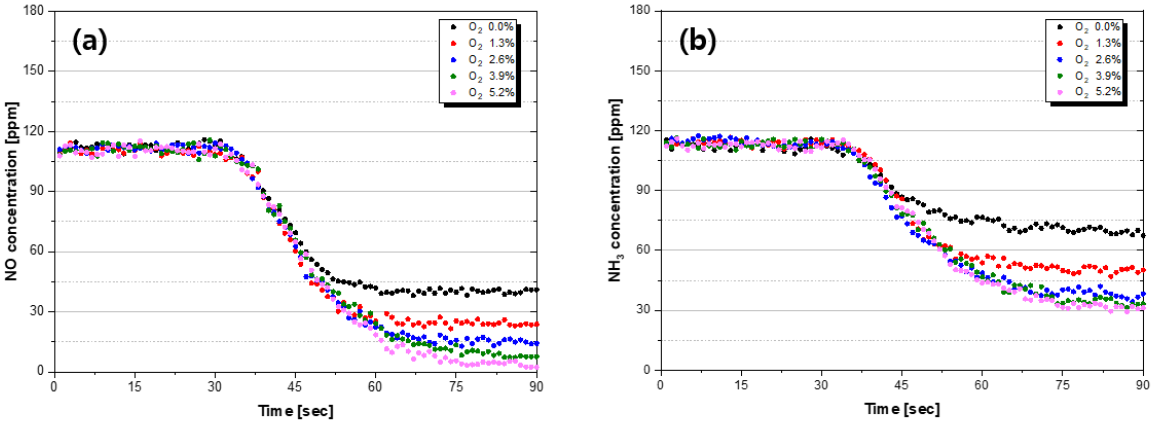

Figure 5: Time evolution of NO and NH_3 concentrations in NO, NH_3, H_2O, O_2, and N_2 mixtures under various initial O_2 concentrations for Case 2 (see Table 1). (Black dot: X_{O2} 0%, red dot: X_{O2} 1.3%, blue dot: X_{O2} 2.6%, green dot: X_{O2} 3.9%, pink dot: X_{O2} 5.2%)

In Case 2, to investigate the effect of the O_3 concentration on photochemical reaction, the experiment was conducted by adjusting the O_2 concentration. In other words, since O_3 is produced by decomposition and a combination reaction of O_2 by UV-C light, the concentration of O_3 can be adjusted according to the injected O_2 concentration. Fig. 5(a) and (b) are experimental results of NO and NH_3 measured according to the concentration of injected O_2, respectively. As the O_2 concentration is increased from 0 to 5.2%, the conversions of NO and NH_3 tend to gradually increase to 64, 79, 87, 93, 95%, and 38, 56, 66, 70, and 72%, respectively. In the case of NH_3, as conversion become similar when the O_2 concentration is higher than 2.6%, there is no significant concentration variations above a specific concentration of O_3. The reason for this result can be inferred as follows: as the O_2 concentration increases, the concentration of O_3 also increases, leading to an increasing conversion of NO through the reactions such as $2NO + O_2 \rightarrow 2NO_2$ and $NO + O_3 \rightarrow NO_2 + O_2$. However, since the H_2O concentration remains constant, the concentration of OH radicals is limited, preventing sufficient occurrence of the reaction described in $NO_2 + \cdot OH + M \rightarrow HNO_3 + M$. Therefore, the availability of HNO_3 required for the reaction in $HNO_3 + NH_3 \rightarrow NH_4NO_{3(s)}$ becomes limited, resulting in NH_3 conversion and reduction showing a converging pattern over time.

As the O_2 concentration increased, the reach time to the steady-state of NO and NH_3 gradually increased. It is estimated that this is due to the increase in the reduced quantity of NO and NH_3 as the concentration of O_3 increases. Even under the condition in which the O_2 concentration was 0% (as indicated by the black dot), which resulted in the absence of O_3, NO and NH_3 showed

https://doi.org/10.5194/egusphere-2025-3602
Preprint. Discussion started: 11 August 2025

conversions of 64% and 38%, respectively. These conversions are caused by OH radicals decomposed from H_2O by UV rays. NO, and OH radicals form $\cdot HONO$, as in the $\cdot OH + \cdot HONO \rightarrow H_2O + NO_2$ and $\cdot OH + NO + M \rightarrow \cdot HONO + M$ reactions, rather than the dominant reaction $NO + O_3 \rightarrow NO_2 + O_2$ during the daytime. Through this process, it is demonstrated that NOx can form HNO_3 even in an environment where O_3 is rare. As these reactions are limited compared to the reaction occurring in an environment where O_3 is sufficient, it is considered that the conversions and reduced quantity of NO and NH_3 are relatively small.

4.4 Effect of relative humidity on NH_4NO_3 formation

In the atmospheric environment, moisture is one of the essential components for the formation of NH_4NO_3. H_2O is decomposed into OH radical through a photolysis reaction or forms HNO_3 through a hydrolysis reaction with N_2O_5 at night. In addition, the growth of hygroscopic particles such as sulfate and nitrate enhances the diameter of the particles and further degrades the visibility rate when the relative humidity increases (Cao et al., 2012). Therefore, a study is required to understand the effect of relative humidity on NH_4NO_3 photochemical reactions in the atmosphere. In Case 3, to control the relative humidity, the flow rate of N_2 supplied to the H_2O bubble generator heated to 350 K was controlled, and accordingly, an experiment was performed to measure the concentration variations of NO and NH_3. Relative humidity and temperature for each condition were measured by a capacitive humidity sensor and PT100 type (TESTO 605i).

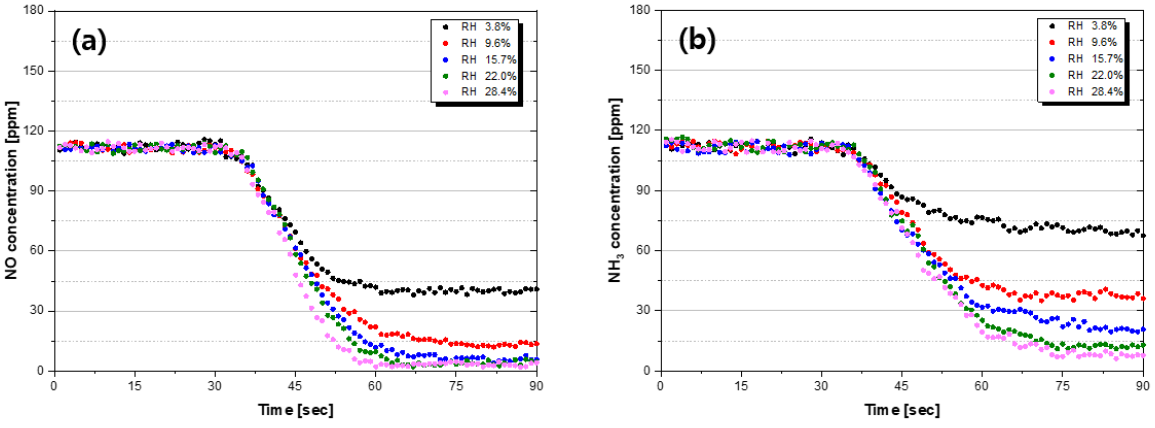

Figure 6: Time evolution of NO and NH_3 concentrations in NO, NH_3, H_2O, O_2, and N_2 mixtures under various relative humidity for Case 3 (see Table 1). (Black dot: RH 3.8%, red dot: RH 9.6%, blue dot: RH 15.7%, green dot: RH 22.0%, pink dot: RH 28.4%)

Fig. 6(a) and (b) present the experimental results measuring the concentration fluctuations of NO and NH_3 according to the relative humidity. When 300 ppmv of NO/N_2, NH_3/N_2 reference gas, purified air, and N_2 passing through the H_2O bubble generator were injected according to each condition in the simulation chamber, relative humidity was measured at 3.8, 9.6,

https://doi.org/10.5194/egusphere-2025-3602
Preprint. Discussion started: 11 August 2025

15.7, 22.0, and 28.4% in sequence. In the case of NO, the conversion proceeded to 64, 88, 95, 96, and 97% as the relative humidity increased, and NH_3 also showed a greater conversion than other conditions, such as UV light intensity or O_3 concentration. As the relative humidity increases, the amount of OH radical converted from H_2O also increases, and the reactions of $\cdot OH + \cdot HONO \rightarrow H_2O + NO_2$ and $\cdot OH + NO + M \rightarrow \cdot HONO + M$ occur actively along with the reaction $NO + O_3 \rightarrow NO_2 + O_2$, producing a large quantity of NO_2. Additionally, it is considered that various reactions, such as $\cdot OH + O_3 \rightarrow \cdot HO_2 + O_2$, $NO_2 + H_2O \rightarrow \cdot HONO$, $NO + NO_2 + H_2O \rightarrow \cdot HONO + \cdot HONO$ and $\cdot HO_2 + NO \rightarrow \cdot OH + NO_2$, interact in combination. Thus, NO_2 forms plenty of HNO_3 because of the $NO_2 + \cdot OH + M \rightarrow HNO_3 + M$ reaction sufficient OH radical concentration, and HNO_3 leads to NH_4NO_3 by reacting with NH_3 like the $HNO_3 + NH_3 \rightarrow NH_4NO_{3(s)}$ reaction.

4.5 Effect of initial NO and NH_3 concentration on NH_4NO_3 formation

NO in the atmosphere is generated during the combustion process from various plants, transportation, and energy systems, and agricultural activities, such as fertilizer and livestock excrement, primarily produce NH_3. This means that a significant amount of NOx is emitted around factories and downtown areas, whereas NH_3 concentrations are high in agricultural and livestock industries. In such environments, the atmospheric chemical mechanisms operate differently, making studying the effect of precursor concentrations necessary.

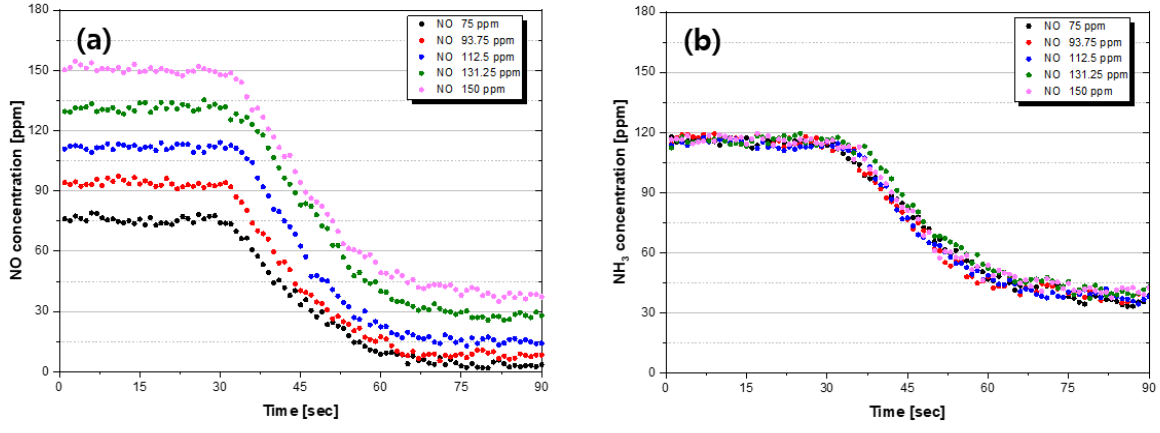

Figure 7: Time evolution of NO and NH_3 concentrations in NO, NH_3, O_2, and N_2 mixtures under various initial NO concentrations for Case 4 (see Table 1). (Black dot: X_{NO} 75 ppmv, red dot: X_{NO} 93.75 ppmv, blue dot: X_{NO} 112.5 ppmv, green dot: X_{NO} 131.25 ppmv, pink dot: X_{NO} 150 ppmv; when X_{NH3} is fixed at 112.5 ppmv)

https://doi.org/10.5194/egusphere-2025-3602
Preprint. Discussion started: 11 August 2025

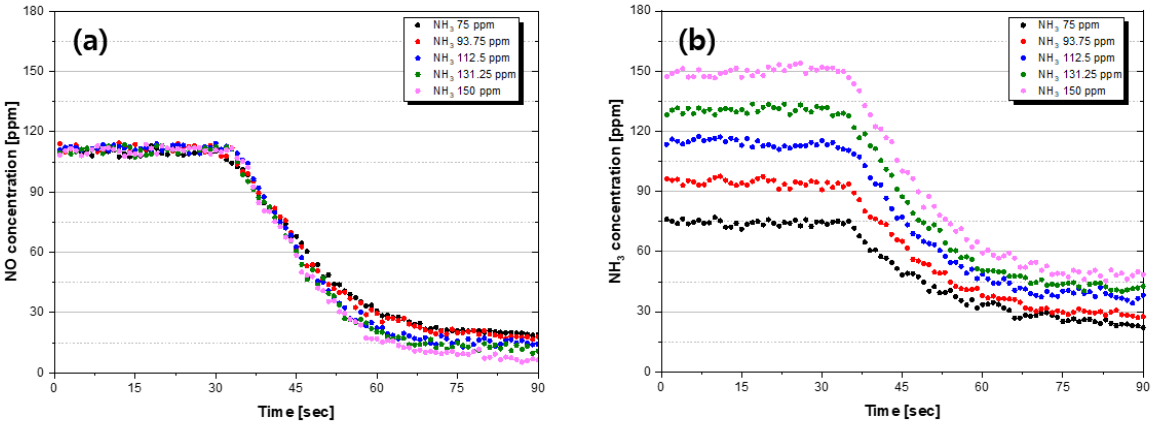

Figure 8: Time evolution of NO and NH_3 concentrations in NO, NH_3, O_2, and N_2 mixtures under various initial NH_3 concentrations for Case 5 (see Table 1). (Black dot: X_{NH3} 75 ppmv, red dot: X_{NH3} 93.75 ppmv, blue dot: X_{NH3} 112.5 ppmv, green dot: X_{NH3} 131.25 ppmv, pink dot: X_{NH3} 150 ppmv; when X_{NO} is fixed at 112.5 ppmv)

In Case 4 and 5, the concentration fluctuations of NO and NH_3 were measured by DAS while controlling the flow rates of NO/N_2 and NH_3/N_2 gases to check how the concentration ratio of NO and NH_3 in the atmosphere affects the formation of NH_4NO_3. Fig. 7(a) and (b) show the changes in NO and NH_3 concentrations when added while increasing the concentration of NO from 75 to 150 ppmv after NH_3 is fixed at 112.5 ppmv. At this time, the NO conversion tends to decrease gradually to approximately 95, 91, 87, 79, and 75%, while the reduction quantity steadily increases. On the other hand, in the case of NH_3, only a constant quantity is converted to about 65%, regardless of the change in NO concentration. Increasing NO concentration, which means a higher amount of NO participation in the $\cdot O + NO + M \rightarrow NO_2 + M$, $2NO + O_2 \rightarrow 2NO_2$ and $NO + O_3 \rightarrow NO_2 + O_2$ reactions, leads to an increased conversion to NO_2. However, in the case of NH_3, it is estimated that the constant concentration of NH_3 is the result of an unaltered HNO_3 amount by the steady concentration of OH radical.

On the contrary, Fig. 8 shows the fluctuations in the concentration of NO and NH_3 when NO is fixed at 112.5 ppmv, and the concentration of NH_3 is controlled from 75 to 150 ppmv. When the ratio of NO and NH_3 concentrations was adjusted to 1:0.67, 0.83, 1, 1.17, and 1.33, the conversion of NO was 82 to 93%, which was a relatively narrow variation, and NH_3 was also 66 to 69%, almost constant. However, the reduction quantity of NH_3 rapidly increases, which is considered to be because as the concentration of NH_3 increases, the quantity of its decomposition into NH_2 by OH radicals increases, as shown in the $\cdot OH + NH_3 \rightarrow H_2O + NH_2$ reaction. As the NH_3 concentration increased, the time required for NO and NH_3 to reach steady state decreased, indicating that higher NH_3 levels can accelerate the conversion process and reaction dynamics.

https://doi.org/10.5194/egusphere-2025-3602
Preprint. Discussion started: 11 August 2025

5 Conclusions

In this study, a detailed exploration of the physicochemical processes underlying NH_4NO_3 formation was conducted under controlled conditions within a small-scale indoor smog chamber. The experimental setup allowed precise manipulation of key environmental variables, including UV-C light intensity, relative humidity, and precursor gas concentrations, facilitating a systematic analysis of their roles in NH_4NO_3 formation. Utilizing real-time laser absorption spectroscopy, we achieved high temporal resolution and accuracy in monitoring the concentration fluctuations of NO and NH_3, essential precursors in the formation process.

The results highlight that UV-C light intensity directly impacts the photochemical reaction rates, with increased light intensity leading to higher photolysis rates and accelerated formation of reactive intermediates such as OH radicals and HNO_3. Relative humidity emerged as a particularly critical factor, significantly enhancing the availability of OH radicals through the photolysis of water vapor, thereby driving secondary aerosol nucleation and growth processes. Our findings reveal that the interaction between relative humidity and UV-C light intensity determines the efficiency of NO and NH_3 conversions and strongly influences the formation and growth rate of NH_4NO_3 particles.

These observations underscore the intricate dependencies of NH_4NO_3 formation on environmental conditions and provide valuable insights into how atmospheric variables modulate secondary aerosol production. By integrating high-sensitivity, real-time monitoring techniques with a controlled experimental framework, this study illuminates the dynamic interplay of precursor gases and environmental factors, advancing our understanding of NH_4NO_3 formation dynamics.

Unlike previous studies that relied on photochemical reaction results in simulation chambers using sampling methods such as chemiluminescence, NDIR, and gas chromatography, this study demonstrated the significant advantages of applying DAS to the real-time monitoring of chemical reactions in the atmospheric environment. The DAS method enabled high-resolution, non-intrusive measurements of NO and NH_3, allowing for the sensitive detection of rapid concentration fluctuations without perturbing the reaction environment. This capability is particularly beneficial for investigating NH_4NO_3 formation, as it reduces uncertainties associated with conventional sampling delays and supports more accurate interpretation of reaction kinetics under varying atmospheric conditions. This approach significantly improves our understanding of complex atmospheric chemical mechanisms by determining the priority of photochemical reactions and estimating the effects of specific environmental factors on acceleration or inhibition. It opens up new avenues for research into the generation and growth of secondary aerosols, providing a powerful tool for future studies in atmospheric chemistry. Future research aims to deepen the understanding of NH_4NO_3 formation mechanisms by integrating quantitative modeling and the detection of intermediate species. This approach seeks to expand the experimental framework and provide more detailed and quantitative insights by incorporating advanced detection techniques and modeling tools.

https://doi.org/10.5194/egusphere-2025-3602
Preprint. Discussion started: 11 August 2025

Author contributions

Conceptualization: NJ, CL; Data processing: SL, DK; Formal analysis: DK, MY; Methodology: NJ, SL; Supervision: SS, CL; Writing (original draft preparation): NJ, MY; Writing (review and editing): SS, CL

Competing interests

The contact author has declared that none of the authors has any competing interests.

Financial support

This work was supported by the Industrial Strategic Technology Development Program - Development of technology of Next-generation Intelligence Semiconductor (20023296, Development of Real-Time Continuous Measurement Equipment for Semiconductor Process Gas Monitoring) funded By the Ministry of Trade, Industry & Energy (MOTIE, Korea).

References

Adopted, I.: Climate change 2014 synthesis report, IPCC: Geneva, Szwitzerland, 2014.

Andersen, S. T., Nelson, B. S., Read, K. A., Punjabi, S., Neves, L., Rowlinson, M. J., Saiz-Lopez, A., Plane, J. M. C., and Carpenter, L. J.: Fundamental oxidation processes in the remote marine atmosphere investigated using the NO–NO2–O3 photostationary state, Atmospheric Chemistry and Physics, 22, 15747-15765, 2022.

Bauer, S., Koch, D., Unger, N., Metzger, S., Shindell, D., and Streets, D.: Nitrate aerosols today and in 2030: a global simulation including aerosols and tropospheric ozone, Atmospheric Chemistry and Physics, 7, 5043-5059, 2007.

Behera, S. N. and Sharma, M.: Degradation of SO2, NO2 and NH3 leading to formation of secondary inorganic aerosols: An environmental chamber study, Atmospheric environment, 45, 4015-4024, 2011.

Butt, E. W., Rap, A., Schmidt, A., Scott, C. E., Pringle, K. J., Reddington, C. L., Richards, N. A. D., Woodhouse, M. T., Ramirez-Villegas, J., Yang, H., Vakkari, V., Stone, E. A., Rupakheti, M., S. Praveen, P., G. van Zyl, P., P. Beukes, J., Josipovic, M., Mitchell, E. J. S., Sallu, S. M., Forster, P. M., and Spracklen, D. V.: The impact of residential combustion emissions on atmospheric aerosol, human health, and climate, Atmospheric Chemistry and Physics, 16, 873-905, 2016.

Cao, J.-j., Wang, Q.-y., Chow, J. C., Watson, J. G., Tie, X.-x., Shen, Z.-x., Wang, P., and An, Z.-s.: Impacts of aerosol compositions on visibility impairment in Xi'an, China, Atmospheric Environment, 59, 559-566, 2012.

Carslaw, N., Creasey, D., Heard, D., Lewis, A., McQuaid, J., Pilling, M., Monks, P., Bandy, B., and Penkett, S.: Modeling OH, HO2, and RO2 radicals in the marine boundary layer: 1. Model construction and comparison with field measurements, Journal of Geophysical Research: Atmospheres, 104, 30241-30255, 1999.

Fuchs, H., Ball, S. M., Bohn, B., Brauers, T., Cohen, R. C., Dorn, H. P., Dubé, W. P., Fry, J. L., Häseler, R., Heitmann, U., Jones, R. L., Kleffmann, J., Mentel, T. F., Müsgen, P., Rohrer, F., Rollins, A. W., Ruth, A. A., Kiendler-Scharr, A., Schlosser, E., Shillings, A. J. L., Tillmann, R., Varma, R. M., Venables, D. S., Villena Tapia, G., Wahner, A., Wegener, R., Wooldridge,

https://doi.org/10.5194/egusphere-2025-3602
Preprint. Discussion started: 11 August 2025

P. J., and Brown, S. S.: Intercomparison of measurements of NO2 concentrations in the atmosphere simulation chamber SAPHIR during the NO3Comp campaign, Atmos. Meas. Tech., 3, 21-37, 2010.

Gordon, I. E., Rothman, L. S., Hill, C., Kochanov, R. V., Tan, Y., Bernath, P. F., Birk, M., Boudon, V., Campargue, A., and Chance, K.: The HITRAN2016 molecular spectroscopic database, Journal of Quantitative Spectroscopy and Radiative Transfer, 203, 3-69, 2017.

Han, S., Bian, H., Feng, Y., Liu, A., Li, X., Zeng, F., and Zhang, X.: Analysis of the relationship between O3, NO and NO2 in Tianjin, China, Aerosol and Air Quality Research, 11, 128-139, 2011.

Kelly, J. T., Parworth, C. L., Zhang, Q., Miller, D. J., Sun, K., Zondlo, M. A., Baker, K. R., Wisthaler, A., Nowak, J. B., and Pusede, S. E.: Modeling NH4NO3 over the San Joaquin Valley during the 2013 DISCOVER-AQ campaign, Journal of Geophysical Research: Atmospheres, 123, 4727-4745, 2018.

Khoder, M.: Atmospheric conversion of sulfur dioxide to particulate sulfate and nitrogen dioxide to particulate nitrate and gaseous nitric acid in an urban area, Chemosphere, 49, 675-684, 2002.

Kim, H., Kang, D., Jung, H. Y., Jeon, J., and Lee, J. Y.: Review of Smog Chamber Experiments for Secondary Organic Aerosol Formation, Atmosphere, 15, 115, 2024.

Lee, S.-B., Bae, G.-N., and Moon, K.-C.: Smog chamber measurements, in: Atmospheric and Biological Environmental Monitoring, Springer, 105-136, 2009.

Qi, X., Zhu, S., Zhu, C., Hu, J., Lou, S., Xu, L., Dong, J., and Cheng, P.: Smog chamber study of the effects of NOx and NH3 on the formation of secondary organic aerosols and optical properties from photo-oxidation of toluene, Science of the Total Environment, 727, 138632, 2020.

So, S., Park, J., Yoo, M., Hwang, J., Kim, D., and Lee, C.: Simultaneous measurement of OH radical, H2O concentration, and temperature in a premixed CH4/air flame using TDLAS with an improved analysis method, Optics Express, 30, 32031-32050, 2022.

Spicer, C. W.: Smog chamber studies of nitrogen oxide (NOx) transformation rate and nitrate precursor relationships, Environmental Science & Technology, 17, 112-120, 1983.

Stelson, A. and Seinfeld, J. H.: Relative humidity and temperature dependence of the ammonium nitrate dissociation constant, Atmospheric Environment (1967), 16, 983-992, 1982.

Stevens, C. J., Dupre, C., Dorland, E., Gaudnik, C., Gowing, D. J., Bleeker, A., Diekmann, M., Alard, D., Bobbink, R., Fowler, D., Corcket, E., Mountford, J. O., Vandvik, V., Aarrestad, P. A., Muller, S., and Dise, N. B.: Nitrogen deposition threatens species richness of grasslands across Europe, Environ Pollut, 158, 2940-2945, 2010.

Tao, W.-K., Chen, J.-P., Li, Z., Wang, C., and Zhang, C.: Impact of aerosols on convective clouds and precipitation, Reviews of Geophysics, 50, 2012.

Zhang, R., Wang, G., Guo, S., Zamora, M. L., Ying, Q., Lin, Y., Wang, W., Hu, M., and Wang, Y.: Formation of urban fine particulate matter, Chem Rev, 115, 3803-3855, 2015.

Zhao, M., Wang, S., Tan, J., Hua, Y., Wu, D., and Hao, J.: Variation of urban atmospheric ammonia pollution and its relation with PM2.5 chemical property in winter of Beijing, China, Aerosol and Air Quality Research, 16, 1378-1389, 2016.